Journal of Nuclear Materials 425 (2012) 8–15

Contents lists available at SciVerse ScienceDirect

Journal of Nuclear Materials

journal homepage: www.elsevier.com/locate/jnucmat

Modeling radiation induced segregation in Ni–Cr model alloys from first principles

L. Barnard [a], J.D. Tucker [b], S. Choudhury [c], T.R. Allen [d], D. Morgan [a,*]

[a] University of Wisconsin-Madison, 1500 Engineering Drive, Madison, WI 53706, USA
[b] Knolls Atomic Power Laboratory, P.O. Box 1072, Schenectady, NY 12301, USA
[c] Los Alamos National Laboratory, 30 Bikini Atoll Rd Los Alamos, NM 87545-0001, USA
[d] University of Wisconsin-Madison, Department of Nuclear Engineering and Engineering Physics, 1500 Engineering Drive, Madison, WI 53706, USA

ARTICLE INFO

Article history:
Available online 24 August 2011

ABSTRACT

In this paper, a rate theory model is employed to study radiation induced segregation (RIS) in Ni–Cr model alloys. In contrast with similar previous models, model parameters have been obtained from first principles via density functional theory (DFT) calculation. Qualitative model behavior is compared and contrasted with the physical mechanisms that underlie conventional RIS models, and the effects of Cr–Cr interstitial trapping and defect sink bias are investigated. It is concluded that: (1) the parameters required in this RIS model are too sensitive to be rigorously determined by present DFT approaches alone, and fitting to experimental RIS data is necessary to produce an accurate model. (2) In contrast with the emphasis of previous RIS models, the best fit DFT-based RIS model suggests that under radiation, the interstitial flux should drive Cr strongly toward enrichment near defect sinks, while the vacancy flux should drive Cr strongly toward depletion, and that the vacancy effect should be slightly stronger resulting in moderate Cr depletion. (3) The effects on RIS of Cr–Cr interstitial trapping and biased defect sinks are relatively small compared with the effects associated with variations in the species dependent diffusivities.

© 2011 Elsevier B.V. All rights reserved.

1. Introduction

Radiation induced segregation is a microstructural process that occurs under radiation whereby an initially homogenous alloy will become demixed [1]. The root cause of this phenomenon is the diffusion of radiation-produced atomic defects to defect sinks, such as grain boundaries. One result of this flux of defects toward defect sinks is the depletion of some alloy components and enrichment of others in the neighborhood of those sinks, with respect to their initial pre-irradiation concentrations. RIS is of particular concern in Cr containing austenitic alloys such as stainless steels or Ni-based super alloys, both of which are ubiquitous in modern light water reactors and are candidate materials for future reactor designs [1,2]. Cr is added to these alloys in part to provide corrosion resistance and experimental results indicate that RIS causes Cr to be depleted near grain boundaries and surfaces, regions where metals are most susceptible to corrosive attack. Corrosion of metallic components in a nuclear power system can lead to failure by a mechanism known as irradiation assisted stress corrosion cracking (IASCC) [1,3], and it is believed that RIS plays an important role in the susceptibility of stainless steels and Ni alloys to IASCC [1,4,5]. A simulation tool that can accurately predict RIS would therefore be valuable for material and reactor design, and potentially for preventative maintenance in existing reactors as well. An additional motivation for studying RIS is that it gives fundamental insights into the nature of point defect mobility, which are at the foundation many aspects of alloy microstructural evolution in nuclear materials.

Many models have been developed to simulate Cr RIS in steels, and most are based on a rate theory approach that numerically solves the coupled diffusion equations of radiation produced defects and alloy components [1]. An early influential model was developed by Perks et al. [6] that presumes that RIS occurs due to preferential vacancy migration with one alloy component relative to the others. In this model, as radiation produced vacancies migrate toward a defect sink, they cause a corresponding net flux of this alloy component away from the defect sink, resulting in depletion of this component in the neighborhood of the sink. This process is the vacancy driven component of the inverse Kirkendall effect. The Perks model also assumes that there is no preferential interstitial migration, thus as radiation produced interstitials migrate toward a defect sink, they carry no net flux of any one alloy component and do not alter the alloy composition near the sink. The most important input parameters for the Perks model are therefore the vacancy diffusivities and compositions for each of the species in the alloy, as these are the parameters that determine which components are enriched or depleted near defect sinks due to RIS. When properly parameterized, such a model can predict RIS with reasonable accuracy at low and

* Corresponding author. Tel.: +1 608 265 5879.
E-mail addresses: lmbarnard@wisc.edu (L. Barnard), tuckjd@kapl.gov (J.D. Tucker), samrat@lanl.gov (S. Choudhury), allen@engr.wisc.edu (T.R. Allen), ddmorgan@wisc.edu (D. Morgan).

0022-3115/$ - see front matter © 2011 Elsevier B.V. All rights reserved.
doi:10.1016/j.jnucmat.2011.08.022

intermediate temperatures; however it is less successful at higher temperatures. An important modification was introduced to this model by Grandjean et al. [7] and developed in detail for the Fe–Ni–Cr alloy system by Allen et al. [8], resulting in the modified inverse Kirkendall model (MIK). This model refines the Perks model by including the effects of local composition on the diffusivities of the alloy species. Compared to the Perks model, the MIK model provides greater fidelity with experimental results, particularly at elevated temperatures and over a much wider range of alloy base compositions. The model parameters used in the MIK model are obtained via fitting to experimental energies and diffusion data, as well as RIS data.

Both the Perks and MIK models were developed and parameterized for fcc based Fe–Ni–Cr alloys, and similar models have been developed to include other species with success [9]. The success of these models demonstrates the robustness and adaptability of this rate theory approach, given suitable input parameters. However, obtaining input parameters from experimental fitting limits the applicability of such models to cases where adequate data is available. Furthermore, the assumption that RIS is determined by only the vacancy diffusivities of the alloy species potentially distorts the physics of the true system, as the interstitial diffusivities of components in an alloy could be very different and potentially play an important role in RIS [10]. Nastar et al. [11] developed a model for RIS in Fe–Ni–Cr alloys that contains additional mechanisms and different parameterizations than the MIK model. First, unlike the MIK model, all the parameters for vacancy diffusion were fit to thermodynamic and diffusion data, and not directly to any RIS data. Contrary to the MIK model, Nastar et al. then found it was necessary to include the contribution of interstitial diffusion to RIS to reproduce experimentally measured segregation. Due to the lack of experimental interstitial diffusion data in Fe–Ni–Cr alloys, the interstitial diffusion parameters in the model of Nastar et al. are obtained via fitting to RIS data. Nastar et al.'s model appears to perform approximately as well as the MIK model in matching RIS data for Fe–Ni–Cr alloys. The MIK model and the model of Nastar et al. thus demonstrate that multiple interpretations of the underlying physics of RIS can result in different models that are equally capable of predicting RIS. Because both models rely to some extent on fitting to RIS data, their capability of accurately modeling RIS data is in itself not sufficient to demonstrate that either model captures the true parameter values or even dominant physical mechanisms of RIS. In this work we explore how *ab initio* density functional theory (DFT) approaches can help clarify the parameter values and mechanisms relevant for RIS in steels.

DFT is a tool that may be used to determine many parameters needed for modeling both vacancy and interstitial diffusion with excellent precision [10,12]. It is possible to develop a RIS model based upon DFT calculations that includes the effects of both interstitial and vacancy diffusion without obtaining parameters from experiments. Such a model may therefore provide new insights or independent corroboration of earlier RIS models that are based on fitting to experimental data. In this study, a versatile model is developed for simulating RIS that is adaptable to general thermodynamic and kinetic frameworks. This model is parameterized exclusively using the DFT-based diffusion parameters of Tucker et al. [10] for the Ni–Cr system. Through the use of *ab initio* parameterization we can avoid *a priori* assumptions regarding the mechanism of RIS, and this model is used to assess the following:

- Is there evidence from DFT calculations that interstitial diffusion plays a significant role in RIS in Ni–Cr alloys?
- Do DFT calculations corroborate the relationship of Ni and Cr vacancy diffusivities established in previous RIS models, and the resulting impact on RIS?
- Can we utilize DFT calculations alone to generate a predictive and well-conditioned RIS model, or will some amount of experimental fitting be required due to the inherent sensitivity of the input parameters of the model?

This article is structured as follows: in Section 2, we will provide a complete description of the model, beginning with the fundamental model rate equations and then detailing the thermodynamic and kinetic parameterization. In Section 3, we will first compare the basic model results with experimental measurements in a Ni–18Cr model alloy. We will then consider two physical phenomena absent from the basic model that may significantly alter model predictions: Cr–Cr interstitial trapping and biased defect sinks. In the concluding section, we will return to the questions posed above, and compare and contrast the qualitative implications of the DFT-based RIS model with the underlying physical mechanisms of previous models.

2. Methods – rate theory model for simulation of RIS

The rate theory RIS model is based on solving the following set of coupled equations to obtain 1-dimensional concentration profiles for each of the species in the simplified system: Ni, Cr, single vacancies, and single interstitials [1,13].

$$\frac{dC_{\mathrm{Ni}}}{dt} = -\frac{dJ_{\mathrm{Ni}}}{dx} \tag{2.1.1}$$

$$\frac{dC_{\mathrm{Cr}}}{dt} = -\frac{dJ_{\mathrm{Cr}}}{dx} \tag{2.1.2}$$

$$\frac{dC_{Vac}}{dt} = \varepsilon K_0 - R_{iv} C_{Vac} C_{Int} - \frac{dJ_{Vac}}{dx} \tag{2.1.3}$$

$$\frac{dC_{Int}}{dt} = \varepsilon K_0 - R_{iv} C_{Vac} C_{Int} - \frac{dJ_{Int}}{dx} \tag{2.1.4}$$

In the above, C_i is the site fraction of species i, J_i is the flux of species i, R_{iv} is the rate coefficient for recombination of vacancies and interstitials, K_0 is the radiation dose rate in dpa/s and ε is the damage efficiency. Throughout this study, we will assume a dose rate of 7×10^{-6} dpa/s and an efficiency of 20%, consistent with 3.2 MeV protons [1]. The radius of recombination is taken to be equal to the first nn distance in fcc Ni. The fluxes J_i are evaluated using the following equations [14]

$$J_{\mathrm{Ni}} = -L^V_{\mathrm{NiNi}} \frac{d\tilde{\mu}_{\mathrm{NiV}}}{dx} - L^V_{\mathrm{NiCr}} \frac{d\tilde{\mu}_{\mathrm{CrV}}}{dx} - L^I_{\mathrm{NiNi}} \frac{d\tilde{\mu}_{\mathrm{NiI}}}{dx} - L^I_{\mathrm{NiCr}} \frac{d\tilde{\mu}_{\mathrm{CrI}}}{dx} \tag{2.1.5}$$

$$J_{\mathrm{Cr}} = -L^V_{\mathrm{CrCr}} \frac{d\tilde{\mu}_{\mathrm{CrV}}}{dx} - L^V_{\mathrm{CrNi}} \frac{d\tilde{\mu}_{\mathrm{NiV}}}{dx} - L^I_{\mathrm{CrCr}} \frac{d\tilde{\mu}_{\mathrm{CrI}}}{dx} - L^I_{\mathrm{CrNi}} \frac{d\tilde{\mu}_{\mathrm{NiI}}}{dx} \tag{2.1.6}$$

$$J_{Vac} = -\left(-L^V_{\mathrm{NiNi}} \frac{d\tilde{\mu}_{\mathrm{NiV}}}{dx} - L^V_{\mathrm{NiCr}} \frac{d\tilde{\mu}_{\mathrm{CrV}}}{dx} - L^V_{\mathrm{CrCr}} \frac{d\tilde{\mu}_{\mathrm{CrV}}}{dx} - L^V_{\mathrm{CrNi}} \frac{d\tilde{\mu}_{\mathrm{NiV}}}{dx} \right) \tag{2.1.7}$$

$$J_{Int} = -L^I_{\mathrm{NiNi}} \frac{d\tilde{\mu}_{\mathrm{NiI}}}{dx} - L^I_{\mathrm{NiCr}} \frac{d\tilde{\mu}_{\mathrm{CrI}}}{dx} - L^I_{\mathrm{CrCr}} \frac{d\tilde{\mu}_{\mathrm{CrI}}}{dx} - L^I_{\mathrm{CrNi}} \frac{d\tilde{\mu}_{\mathrm{NiI}}}{dx} \tag{2.1.8}$$

where L^k_{ij} is the phenomenological coefficient relating the flux of species i to a driving force acting on species j through diffusion of defect species k. The driving forces for diffusion are written here as the gradient in diffusion potentials [14,15], defined as

$$\begin{aligned} \tilde{\mu}_{iV} &= \mu_i - \mu_{Vac} \\ \tilde{\mu}_{iI} &= \mu_i + \mu_{Int} \end{aligned} \tag{2.1.9}$$

where μ_i is the chemical potential of species i.

We apply the above set of equations to a physical system that consists of a one dimensional, semi-infinite fcc Ni crystal with an ideal free surface on one side, which acts as a sink for the radiation induced vacancies and interstitials. To treat this system numerically, we bin the system by lattice planes and evaluate the site fraction of each species in each lattice plane. The gradients of fluxes and diffusion potentials in (1–8) then become finite difference equations, as follows:

$$\frac{dJ_i^n}{dx} = -\left[\frac{J_i^{n+1} - J_i^n}{\Delta x}\right]$$
$$\frac{d\tilde{\mu}_i^n}{dx} = \left[\frac{\tilde{\mu}_i^n - \tilde{\mu}_i^{n-1}}{\Delta x}\right] \quad (2.1.10)$$

where $\tilde{\mu}_i^n$ is the diffusion potential of species i in plane n, J_i^n is the flux of species i between plane $n-1$ and n, and Δx is the interplanar distance between adjacent {1 1 1} planes in a Ni crystal.

We solve the resulting set of finite difference equations subject to the following set of boundary conditions [1]. Plane 1 of the system is the first lattice plane and is modeled as an ideal flat surface that cannot exchange atoms with the adjacent vacuum, which places the following constraint on Ni and Cr in the first plane:

$$J_{\mathrm{Ni,Cr}}^1 = 0 \quad (2.1.11)$$

The surface is modeled as an ideal defect sink, which maintains the concentration of vacancies and interstitials in plane 1 at their thermodynamic equilibrium values. This imparts the following condition on defect species in the first plane:

$$\frac{dC_{Vac,Int}^1}{dt} = 0 \quad (2.1.12)$$

The deep boundary represents a plane near enough to the center of a grain in the material that the net flux of any species is approximately zero. This boundary is treated with a mirror boundary condition:

$$J_i^{DB} = 0 \quad (2.1.13)$$

For the initial condition of the system, we set the concentration of the vacancies and interstitials in all planes equal to their bulk thermal equilibrium concentrations as determined by DFT calculations, and we set the Ni and Cr concentrations equal to their nominal alloy compositions. We then evolve the system in time using a modified implicit multistep Newton method, implemented using the DLSODE solver package [16].

The thermodynamic components of the model equations are contained within the chemical potential terms μ_i. Following the derivation of Lupis [17] it is possible to derive a set of chemical potentials for each species in the system from an arbitrary expression of the Gibbs free energy, provided that it is a function only of the composition of the system. For the system of Ni, Cr, Vac, and Int, the resulting expressions are

$$\mu_{Ni} = G_m - C_{\mathrm{Cr}}\frac{\partial G_m}{\partial C_{\mathrm{Cr}}} - C_{Vac}\frac{\partial G_m}{\partial C_{Vac}} - C_{Int}\frac{\partial G_m}{\partial C_{Int}} \quad (2.1.14)$$

$$\mu_{\mathrm{Cr}} = G_m + (1 - C_{\mathrm{Cr}})\frac{\partial G_m}{\partial C_{\mathrm{Cr}}} - C_{Vac}\frac{\partial G_m}{\partial C_{Vac}} - C_{Int}\frac{\partial G_m}{\partial C_{Int}} \quad (2.1.15)$$

$$\mu_{Vac} = G_m - C_{\mathrm{Cr}}\frac{\partial G_m}{\partial C_{\mathrm{Cr}}} + (1 - C_{Vac})\frac{\partial G_m}{\partial C_{Vac}} - C_{Int}\frac{\partial G_m}{\partial C_{Int}} \quad (2.1.16)$$

$$\mu_{Int} = G_m - C_{\mathrm{Cr}}\frac{\partial G_m}{\partial C_{\mathrm{Cr}}} - C_{Vac}\frac{\partial G_m}{\partial C_{Vac}} + (1 - C_{Int})\frac{\partial G_m}{\partial C_{Int}} \quad (2.1.17)$$

where G_m is the partial molar Gibbs free energy of the system. For this study, we will utilize the following expression for the free energy:

$$G_m = C_{\mathrm{Cr}}C_{Vac}W_{\mathrm{Cr}Vac} + C_{\mathrm{Cr}}C_{Int}W_{\mathrm{Cr}Int} + C_{Vac}E_{Vac} + C_{Int}E_{Int} + k_bT\sum_i C_i \ln C_i \quad (2.1.18)$$

where C_i is the mole fraction of species i, E_i is the formation energy of defect species i, W_{ij} is the 1st nn interaction parameter of species i and j. E_i and W_{ij} are calculated by DFT [10]. This thermodynamic model is consistent with the calculation of the dilute alloy tracer diffusion coefficients as described in [10], which include the effects of Cr-vacancy and Cr-interstitial binding.

The diffusion kinetics of the model system are contained in the phenomenological coefficients L_{ij}. Because the results of [10] include values of L_{ij} only in the dilute limit, we utilize a method for approximating the phenomenological coefficients as a function of composition provided by the Manning random alloy theory [18], which was derived for systems which may be approximated as solid solutions, and should be appropriate for Ni–Cr alloys in the temperature range of interest to RIS. Based on the Manning model the concentration dependent phenomenological coefficients can be expressed in terms of the tracer diffusion coefficients (assumed constant with composition) as:

$$L_{ii} = \left(\frac{C_iD_i^*}{k_bT}\right)\left(1 + \frac{(1-f_0)}{f_0}\frac{C_iD_i^*}{\sum_m C_mD_m^*}\right)$$
$$L_{ij} = L_{ji} = \frac{(1-f_0)}{f_0}\left(\frac{C_iC_jD_i^*D_j^*}{k_bT\sum_m C_mD_m^*}\right) \quad (2.1.19)$$

where C_i is the concentration of species i, f_0 is a correlation factor for diffusion, and D_i^* is the tracer diffusion coefficient of species i as calculated by the method detailed in [10]. Although Eq. (2.1.19) were derived for vacancy diffusion, a very similar derivation for interstitial diffusion is provided in [19]. The resulting expressions are identical to Eq. (2.1.19), except that the interstitial tracer diffusivities from [10] and the interstitial correlation factor are used instead of the vacancy counterparts.

The use of composition-independent diffusion coefficients places this model at a similar level of approximation as the Perks model. While the MIK model showed a clear improvement in accuracy through the inclusion of compositional dependence in the diffusion coefficients, Perks et al. demonstrated that a model based on diffusion coefficients that are constant with respect to composition could qualitatively capture RIS phenomena in many austenitic alloys reasonable well. The MIK model demonstrated that composition-dependent diffusion coefficients are essential for accurately simulating RIS in austenitic alloys across varying base alloy compositions with a single set of parameters. Neglecting these compositional effects by using compositionally-independent D_i^* values in Eq. (2.1.19) will therefore limit the applicability of this DFT-based model with respect to the MIK model or other composition dependent models, e.g., the model of Nastar et al. [11].

To simulate RIS, we use the chemical potentials provided by Eqs. (2.1.14)–(2.1.18) and the phenomenological coefficients provided by Eq. (2.1.19) to parameterize the flux Eq. (2.1.15)–(2.1.18). We then use these flux equations to solve the rate Eqs. (2.1.1)–(2.1.4) according to the finite difference method and boundary conditions provided in Eqs. (2.1.10)–(2.1.13).

3. Results and discussion

3.1. RIS model predictions in a Ni–18Cr Alloy

Fig. 1 depicts the simulated RIS concentration profiles for a Ni–18Cr model alloy. The model predicts Cr enrichment at all temperatures, contrary to experimental results for this alloy [20]. Figs. 2 and 3 depict Cr segregation as a function of dose and temperature, respectively, as well as experimental results [20]. For these

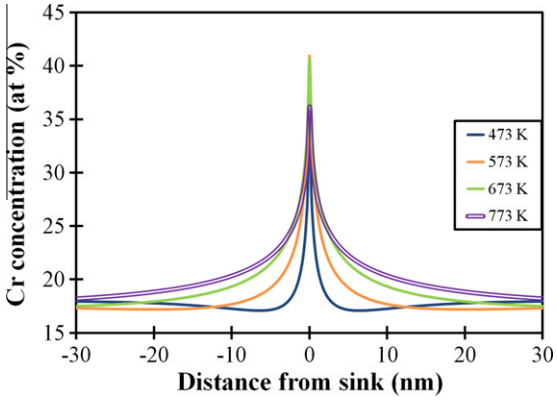

Fig. 1. Model Cr RIS profiles at 0.5 dpa for 473 K–773 K.

and all other figures, Cr segregation is defined as the difference between the concentration at the sink and the nominal alloy concentration, where a positive value indicates enrichment and a negative value indicates depletion. The Cr sink concentration is defined as the average Cr concentration in a 2 nm region about the sink. This value differs from the Cr concentration in the sink plane by 1–2% and is intended to provide an approximation of the finite measurement width effects that occur in experimental RIS measurements by STEM or AES [21]. With this RIS model certain features of the RIS phenomenon are accurately captured, such as steady state dose and maximum RIS temperature, however the sign of the predicted segregation does not agree with experimental measurement.In the Ni–18Cr alloy, the RIS model erroneously predicts Cr enrichment. This result is due to the dominance of fast Cr interstitial diffusion in the model. The relative contributions of vacancies and interstitials may be clarified by investigating the effects of interstitial and vacancy diffusion on RIS in the Ni–18Cr alloy separately. The effect of one type of defect may be isolated by setting the Ni and Cr diffusivities of the other type of defect equal to one another. For example, to isolate the effect of interstitial diffusion on RIS, we set D_{Cr}^{*Vac} equal to D_{Ni}^{*Vac} (or equivalently, $D_{Cr}^{*Vac}/D_{Ni}^{*Vac} = 1$). While the magnitudes of D_{Cr}^{*Vac} and D_{Ni}^{*Vac} will have a modest influence on the extent of Cr RIS, with this constraint the sign and the magnitude of the Cr segregation are determined predominantly by the ratio $D_{Cr}^{*Int}/D_{Ni}^{*Int}$. An analogous operation is performed to isolate the effect of vacancy diffusion. Fig. 4 depicts the Cr concentration profiles at 673 K and 0.5 dpa produced by the isolated mechanisms of interstitial and vacancy diffusion, as well as the profile produced by their aggregate effects. Vacancy diffusion clearly leads to Cr depletion, while interstitial diffusion causes Cr enrichment. When

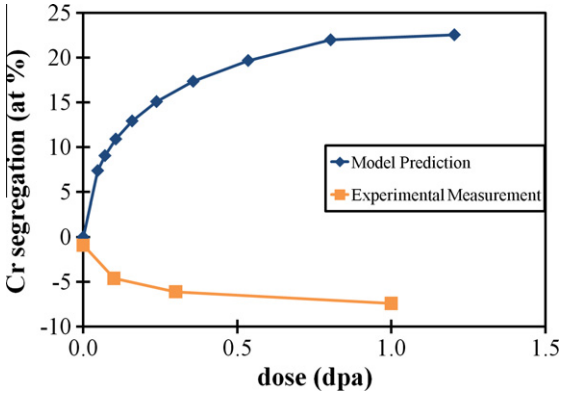

Fig. 2. Model predicted and experimentally measured [20] Cr segregation at 673 K as a function of dose.

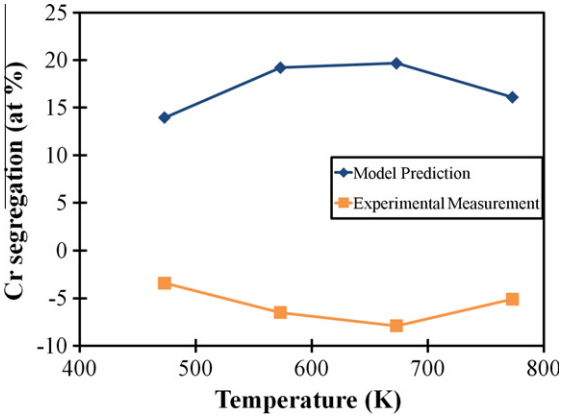

Fig. 3. Model predicted and experimentally measured [20] Cr segregation at 0.5 dpa as a function of temperature.

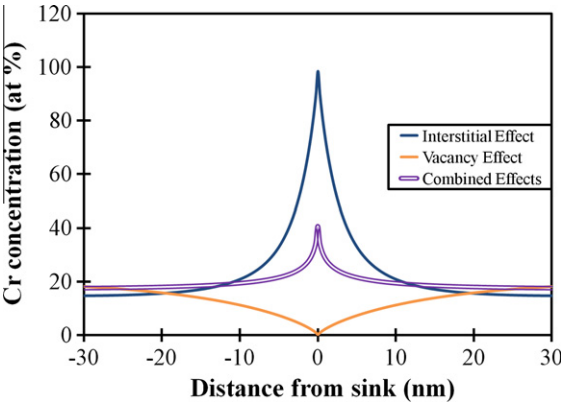

Fig. 4. Model predicted Cr profiles at 0.5 dpa and 673 K for the isolated effects of interstitial and vacancy diffusion, as well as their combined effect.

their effects are combined, interstitial diffusion dominates and results in overall Cr enrichment in this set of model calculations.Fast Cr diffusion by vacancies is often cited as the dominating effect that causes Cr depletion during RIS in fcc Ni and Fe alloys [6,8], and adjusting the ratio $D_{Cr}^{*Int}/D_{Ni}^{*Int}$ to be equal to 1 produces the RIS profile that results from vacancy diffusion alone. However, it is evident from Fig. 4 that, using the values from Ref. [10], invoking the vacancy effect alone results in complete Cr depletion at the sink, whereas much milder Cr depletion is observed experimentally [20].The DFT-based RIS model presented here produces qualitatively inaccurate RIS predictions, and we have considered possible sources of this significant discrepancy. First, we investigated the potential role of errors in the DFT calculations used to determine the Cr vacancy and interstitial diffusivities used in the model (the diffusion energetics for Ni seem to agree well with experiments [10] so we focus on possible errors associated with Cr). In the multifrequency approach used in [10], both D_{Cr}^{*Int} and D_{Cr}^{*Vac} are functions of several distinct migration barriers. To determine whether errors in the determination of these migration barriers can fully account for the discrepancy between model prediction and experimental measurement, we selected four of the vacancy migration frequencies (following the conventions of [10] denoted w_1, w_2, w_3, w_4) and four of the interstitial migration frequencies (w_R, w_I, w_3, w_2') and treated their associated migration barriers as adjustable parameters. These barriers were selected because they have the most significant impact on the Cr vacancy and interstitial diffusivities. We then fit these barriers through a

least-squares optimization of the difference between the model results and the experimental Cr segregation measurements at 473 K, 573 K, 673 K, and 773 K [20], using the original DFT values from Ref. [10] as the initial guesses for these parameters. As we are fitting eight parameters with only four data points, the resulting fit will likely not be unique. However, by using the DFT values as initial guesses, we can determine how much these barriers would need to change to bring the model into agreement with experiment, and whether this change is within the expected error of the DFT calculations from [10]. The resulting best-fit model is physically identical to the multifrequency models of [10]; the only difference is that the migration barriers of the eight abovementioned frequencies are treated as adjustable parameters, rather than using the values calculated by DFT.

Fig. 5 depicts experimentally measured Cr segregation as a function of temperature as well as the results of the best-fit model. While the agreement with experiment at low temperatures is much better after fitting, the turnaround in RIS behavior at higher temperature is not captured by the basic model. The MIK model invokes a locally reduced vacancy formation enthalpy at the sink, which helps significantly in capturing this effect. Including this effect and using the sink vacancy formation enthalpy of 1.4 eV as recommended in Ref. [20] results in improved model agreement with experimental measurement. The DFT calculated values of the eight adjustable migration barriers and their values in the best fit model of Fig. 5 are summarized in Table 1. The largest difference between the DFT calculated values and the best fit values is 0.037 eV, while the error in the DFT values associated with convergence alone was estimated in Ref. [10] to be 0.035 eV. Thus, it is possible to bring the model predictions into agreement with experimental measurement by adjusting some of the input parameters by an amount commensurate with the expected error in the DFT parameters.

Fig. 6 depicts the ratios $D_{Cr}^{*Vac}/D_{Ni}^{*Vac}$ and $D_{Cr}^{*Int}/D_{Ni}^{*Int}$ as a function of temperature for both the best fitted model and as determined by DFT in Ref. [10]. It is important to note that even after adjusting the model input parameters to reproduce experimental data, the tracer diffusivity ratios for vacancy and interstitials still reflect the primary conclusions reached in Ref. [10]; namely, that Cr diffuses much faster by both vacancies and interstitials, and the final RIS behavior is the result of the competition between these effects. Consequently, there is some evidence from this model that interstitials play a significant role in RIS. However contrary to the model of Nastar et al. [11] the effect of interstitials in this model leads to Cr enrichment, rather than Ni enrichment. Furthermore, the DFT-based RIS model suggests that the disparity between the Cr and Ni vacancy diffusivities is much larger than has been proposed in all previous RIS models of which we are aware. Therefore, rather than corroborating one or more of the previously established Ni–Cr RIS models, the model developed here represents a significantly different physical description of the mechanisms underlying RIS.

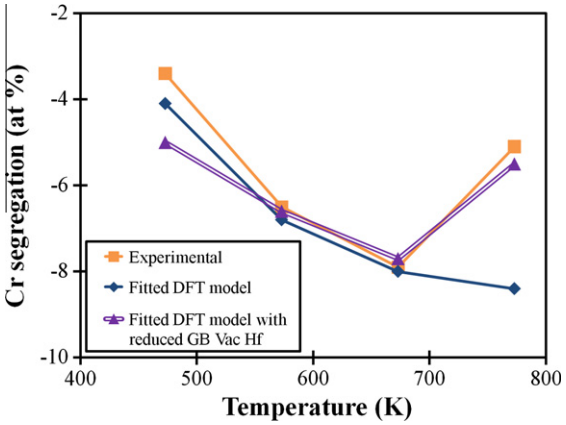

Fig. 5. Cr segregation at 0.5 dpa from experimental measurement, from the best fit model, and the best fit model including the effect of reduced GB enthalpy of formation.

In the next section, we will consider two additional physical phenomena absent from the basic DFT-based RIS model that may also contribute to the discrepancy between model predictions and experimental measurements: Cr–Cr interstitial trapping and biased defect sinks.

3.2. RIS model predictions with Cr–Cr interstitial trapping and biased defect sinks

Independent of the ratios $D_{Cr}^{*Vac}/D_{Ni}^{*Vac}$ and $D_{Cr}^{*Int}/D_{Ni}^{*Int}$, the RIS model predictions can be altered by reducing the flux of one type of defect with respect to the other. In this section we will consider two phenomena that may reduce the interstitial flux, thereby inhibiting the effect of interstitials on RIS and strengthening the effect of vacancies. The first phenomenon is Cr–Cr interstitial trapping. Interstitials are known to bind strongly to Cr solutes in Ni-based fcc alloys [22]. The strong binding between a single Cr and an interstitial (in a local environment of pure Ni) is already accounted for in the calculation of the diffusivities [10] and the formulation of the system free energy (Section 2.2). However, Cr–Cr interactions are not included in the dilute model of Ref. [10] and have been shown to be significant [22], and it was suggested by Tucker et al. [10] that the loss of mobile interstitials as they become trapped as strongly bound Cr–Cr interstitial dumbbells could have a significant impact on RIS. The second phenomenon we will consider is the effect of biased microstructural defect sinks, such as dislocations, which preferentially capture interstitials [1,23]. We will note here that a third phenomenon which may alter the balance of vacancies and interstitials is defect production bias [1]. During irradiation damage cascades both interstitials and vacancies can form immobile defect clusters, and there is evidence from experiment [24] and simulations [25] that more interstitials are lost to these clusters than vacancies, resulting in an unbalanced effective production rate of mobile defects. The possibility of such a production bias playing a role in RIS has been mentioned in both Refs. [10,12]. However, production bias is a phenomenon that occurs only when defects are produced in cascades, and does not occur when defects are produced as single Frenkel pairs, such as under electron irradiation. If production bias has a substantial effect on RIS, one would therefore expect RIS behavior to depend strongly on irradiation type. Such a dependence is not observed experimentally, as similar alloys irradiated with electrons [26] and protons [20] exhibit very similar segregation. These results suggest that production bias does not play a significant role in RIS and we will therefore not consider it further here.

In reality, some fraction of the excess vacancies that result from the loss of interstitials to biased sinks cluster together to form voids rather than diffusing to a grain boundary. For example, .the interstitial dislocation bias is often linked to radiation-induced swelling in fcc metals [1] associated with void formation. However, in our models we will assume that all excess vacancies diffuse to the sink plane, thereby providing an approximation for the maximum impact of the effects being considered on RIS. In the model any process that suppresses the interstitials and leaves excess vacancies results in a flux of excess vacancies to the sink plane with respect to interstitials, and there is a corresponding small net loss of mass in the sink plane:

$$\frac{dC_{Cr}^{1}}{dt}+\frac{dC_{Ni}^{1}}{dt}<0=K_{loss} \tag{3.2.1}$$

In a physical system, we hypothesize that these excess vacancies would diffuse along the grain boundary and ultimately coalesce into grain boundary voids or be annihilated at surface

Table 1
Values of the eight migration barriers used as adjustable parameters in the best fit model as calculated in [10] by DFT, values used in the best fit model of Fig. 5, and the absolute difference between the two values.

Vacancy barrier	DFT value (eV)	Fitted value (eV)	Absolute difference (eV)	Interstitial barrier	DFT value (eV)	Fitted value (eV)	Absolute difference (eV)
w_1	0.980	0.943	0.037	w_R	0.750	0.735	0.015
w_2	0.828	0.821	0.007	w_1	0.310	0.345	0.035
w_3	1.018	0.988	0.030	w_3	0.260	0.285	0.025
w_4	1.054	1.061	0.007	w_2'	0.000	0.016	0.016

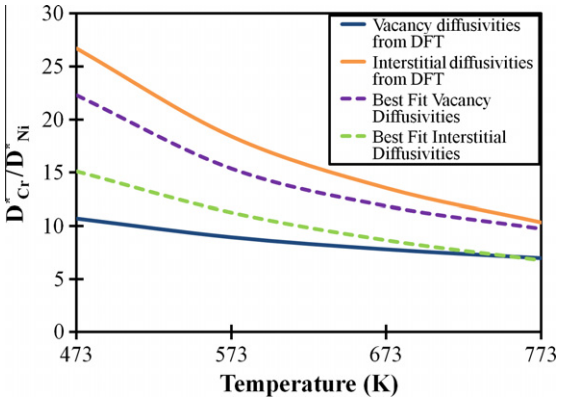

Fig. 6. Cr and Ni tracer diffusivity ratios as calculated by DFT in [10] and as calculated using the best fit model parameters in Table 1.

sinks. Mass balance in the first lattice plane is then restored by the flux of atoms corresponding to this diffusion of vacancies along the grain boundary to other sinks. To simulate this atom flux, we add the following terms to the concentration evolution of atomic species in the first lattice plane:

$$\frac{dC^1_{Cr}}{dt} \rightarrow \frac{dC^1_{Cr}}{dt} + K_{Cr}$$
$$\frac{dC^1_{Ni}}{dt} \rightarrow \frac{dC^1_{Ni}}{dt} + K_{Ni} \quad (3.2.2)$$

where the restoration rates K_{Cr} and K_{Ni} are defined such that they balance the total loss rate K_{loss}:

$$K_{Cr} + K_{Ni} = -K_{loss} \quad (3.2.3)$$

If the restoration of mass occurs via grain boundary diffusion, then it is reasonable to suppose that these rates are proportional to the near grain boundary concentrations of Cr and Ni. This constraint combined with the fact that $C^1_{Cr} + C^1_{Ni} \approx 1$ and Eq. (3.2.3) yields

$$K_{Cr} = -C^1_{Cr} K_{loss}$$
$$K_{Ni} = -C^1_{Ni} K_{loss} \quad (3.2.4)$$

We now consider the necessary alterations to the basic DFT-based RIS model to implement the effect of Cr–Cr interstitial trapping. This approach follows that given in Ref. [27]. The traps in the RIS model are selected to be pairs of Cr atoms sitting on a lattice as nearest-neighbors. When a migrating interstitial dumbbell encounters such a trap, it will form a Cr–Cr dumbbell, which is a very stable defect configuration in dilute Ni–Cr alloys. If the Cr concentration is below the percolation threshold, a Cr–Cr interstitial dumbbell must first dissociate from one Cr atom to form a Ni–Cr dumbbell and then again to form a Ni–Ni dumbbell before it can resume long range diffusion. If the energy required for these dissociations is sufficiently high, the Cr–Cr dumbbell configuration may serve as a temporary trap for interstitials. The energy landscape of dissociation is such that minimum energy to completely dissociate a Cr–Cr dumbbell is the binding enthalpy, 0.92 eV [22]. This trapping mechanism is implemented by introducing two new defect species into our rate model: trapped Cr–Cr interstitials and unoccupied Cr interstitial traps, defined as any Cr with at least one Cr in a nearest neighbor position. The equations that describe the time evolution of these new species are

$$\frac{dC^T_{Int}}{dt} = K^T_{Int} C^T C_{Int} - \tau_{Int} C^T_{Int} - R^T_{Int} C^T_{Int} C_{Vac}$$
$$\frac{dC^T}{dt} = -K^T_{Int} C^T C_{Int} + \tau_{Int} C^T_{Int} + R^T_{Int} C^T_{Int} C_{Vac} \quad (3.2.5)$$

where C^T_{Int} is the concentration of trapped interstitials and C^T is the concentration of unoccupied traps. R^T_{Int} and K^T_{Int} are the recombination and trapping coefficients, respectively given by

$$R^T_{Int} = \frac{4\pi r_{VT}}{\Omega} D_{Vac}$$
$$K^T_{Int} = \frac{4\pi r_{IT}}{\Omega} D_{Int} \quad (3.2.6)$$

where r_{VT} is the recombination radius for a vacancy and a trapped interstitial, given by the normal vacancy-interstitial recombination radius, and r_{IT} is the trapping radius, equal to the 3rd nearest neighbor distance. The dissociation coefficient τ_{Int} determines how strongly interstitials are bound to traps, and is given by

$$\tau_{Int} = \frac{D_{Int}}{a^2} \exp\left[\frac{-E_{bind}}{k_b T}\right] \quad (3.2.7)$$

where E_{bind} is the binding enthalpy of the trap. Note that only one of the two equations in Eq. (3.2.5) needs to be solved, as the two new trapping species are trivially related by

$$C^T = C^T_0 - C^T_{Int} \quad (3.2.8)$$

Here C^T_0 is the initial concentration of unoccupied traps, approximated by the number of Cr–Cr nearest neighbor pairs assuming a random distribution on an fcc lattice. A probability calculation yields the expression

$$C^T_0 = C_{Cr}(1 - C^z_{Ni}) \quad (3.2.9)$$

C_{Cr} and C_{Ni} are the nominal alloy concentrations of Cr and Ni, and the power $z = 12$ is the number of nearest-neighbors in the fcc lattice.

The introduction of the trapping species requires the following alterations to the continuity equations for vacancies and (unbound) interstitials:

$$\frac{dC_{Vac}}{dt} = \varepsilon K_0 - R_{IV} C_{Int} C_{Vac} - R^T_{Int} C^T_{Int} C_{Vac} - \frac{dJ_{Vac}}{dx}$$
$$\frac{dC_{Int}}{dt} = \varepsilon K_0 - R_{IV} C_{Int} C_{Vac} - K^T_{Int} C^T C_{Int} + \tau_{Int} C^T_{Int} - \frac{dJ_{Int}}{dx} \quad (3.2.10)$$

The new terms are the recombination rate of vacancies with trapped interstitials $R^T_{Int} C^T_{Int} C_{Vac}$, the loss rate of free interstitials to traps $K^T_{Int} C^T C_{Int}$, and the release rate of trapped interstitials $\tau_{Int} C^T_{Int}$.

In Fig. 7, the bulk concentration evolution of freely migrating interstitials is plotted both with and without the effects of interstitial binding. Evidently the primary effect of Cr interstitial trapping is to temporarily suppress the buildup of mobile radiation-induced interstitials in the bulk. Eventually, however, the rate of interstitial loss to trapping becomes equal to the rate at which trapped interstitials manage to escape, at which time build up of interstitials proceeds rapidly. The final steady state interstitial concentration is only slightly reduced with respect to the system with no interstitial trapping.

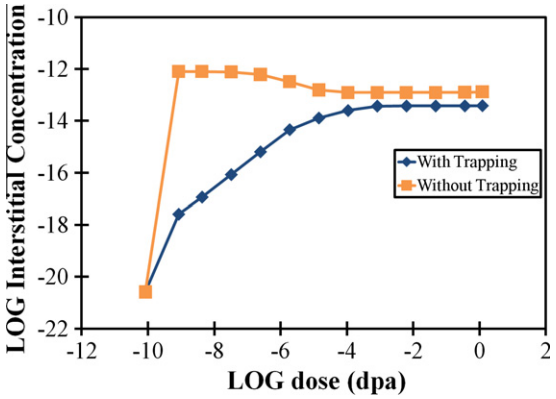

Fig. 7. Model predicted bulk interstitial concentration at 673 K with and without trapping as a function of dose.

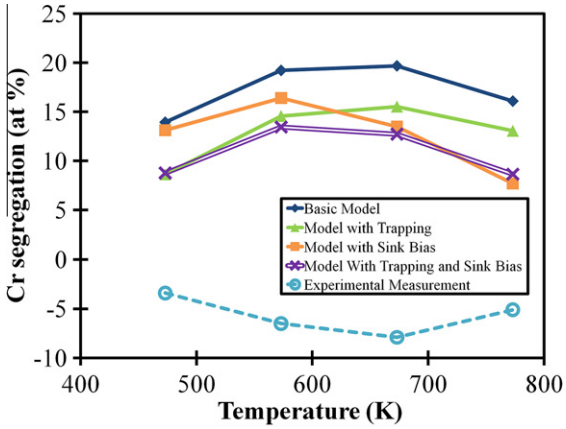

Fig. 8. Cr segregation at 0.5 dpa as a function of temperature for four scenarios: The basic model, the model with trapping, the model with biased sinks, and the model with both trapping and biased sinks. Experimental measurements from [20] are included as well.

To implement the effect of biased defect sinks, the following alterations to concentration evolution equations for interstitials and vacancies (Eqs. (2.1.3), (2.1.4)) are necessary:

$$\frac{dC_{Vac}}{dt} = G - R_{IV}C_{Int}C_{Vac} - R_{VD}C_{Vac} - \frac{dJ_{Vac}}{dx}$$
$$\frac{dC_{Int}}{dt} = G - R_{IV}C_{Int}C_{Vac} - R_{ID}C_{Int} - \frac{dJ_{Int}}{dx} \quad (3.2.11)$$

The new terms associated with loss to dislocations are $R_{VD}C_{Vac}$ and $R_{ID}C_{Int}$, which describe the rate of vacancy and interstitial loss to dislocations, respectively. The rate coefficient R_{jD} is determined by the following equation [1]:

$$R_{jD} = Z_{jD}4\pi r_{iD}\frac{\rho_D}{d}D_j \quad (3.2.12)$$

where r_{jD} is the radius of capture for defect species j, r_D is the dislocation density, d is the interplanar distance, and D_j is the diffusivity of defect species j. The biased defect loss is captured by the bias factor Z_{jD}, where $Z_{jD} > 1$ results in biased loss of defect species j.

RIS was simulated in the Ni–18Cr model alloy using a constant dislocation density of 10^{12} m/m^3, a reasonable value for an annealed fcc metal [28]. The self-interstitial dislocation bias in Ni has been estimated by Wolfer to be as high as approximately 1.3 [23]. While this value is higher than more generally accepted values in the range of 1.1–1.2 [1], we will utilize it in this analysis to provide an upper bound for the effect of sink bias.

Fig. 8 depicts the DFT-based model predicted Cr segregation at 0.5 dpa as a function of temperature for four different scenarios: first, using only the basic model, second, including the effects of interstitial trapping, third, including biased sinks, and finally, including both trapping and biased sinks. While both trapping and biased sinks result in reduced Cr enrichment relative to the basic model, their effects, even when combined, are insufficient to bring the model prediction into agreement with experiment.

4. Conclusions

We have constructed a general rate theory based RIS model that is parameterized with DFT calculations from [10]. This model was used to study RIS in a Ni–18Cr model alloy and predicts strong Cr enrichment, which is in qualitative disagreement with experimental results. This discrepancy was attributed to preferential Cr interstitial diffusion in the model, which overpowered the effect of the preferential Cr vacancy diffusion and lead to overall Cr enrichment.To assess the possible impact of errors in the determination of the model input parameters on the discrepancy between the model prediction and experimental results, eight migration barriers used in [10] to determine D_{Cr}^{*Vac} and D_{Cr}^{*Int} were treated as fitting parameters and adjusted from their DFT values until the model produced RIS results in agreement with experiment. It was necessary to adjust the original DFT parameter values by only 0.037 eV or less to bring the model into agreement with experiment, which is commensurate with the DFT convergence error of 0.035 eV estimated for these parameters [10]. This fit was underconstrained and therefore not unique, but it does indicate that the model can traverse a wide spectrum of RIS behavior from strong Cr enrichment to depletion simply by adjusting the input parameters by an amount similar is magnitude to their DFT error bars.

The best fit model suggests the following mechanism for RIS: under irradiation, the interstitial flux strongly drives Cr enrichment, while the vacancy flux strongly drives Cr depletion. The balance is tipped slightly in favor of the vacancy flux, resulting in moderate Cr depletion. This understanding is a significant departure from previous RIS models, which suggest that the vacancy flux causes moderate Cr depletion and the interstitial flux either plays no role in RIS [6,8] or that interstitials cause additional Cr depletion [11,29].

Returning to the questions posed in Section 1, we conclude the following:

- Both the basic DFT-based RIS model and the best fit RIS model indicate that interstitials should play an important role in RIS in Ni–Cr alloys. However, contrary to previous RIS models which suggest that interstitials should drive Ni enrichment, the model developed in this study indicates that interstitials should drive Cr enrichment.
- The DFT-based RIS model developed here qualitatively matches the relationship between the Ni and Cr vacancy diffusivities that underlies previous RIS models but there are significant quantitative discrepancies. Specifically, the model developed in this study suggests that the depletion caused by the vacancy driven component of the inverse Kirkendall effect should be much stronger than predicted by previous models.
- The fitting exercise in Section 3.1 indicates that the input parameters for this model are extremely sensitive, even compared with the generally good accuracy of DFT calculations. In addition, errors associated with the intrinsic accuracy of DFT and additional complexities hard to treat in DFT (e.g., concentration effects for higher Cr content) will further exacerbate the challenges of obtaining quantitative DFT based RIS models. It is therefore unlikely refining the DFT calculations used in the present model to reduce convergence error will be sufficient to eliminate the discrepancy between the model prediction and

experimental RIS measurements. Consequently, some amount of fitting to experimental RIS data is still necessary to produce an accurate RIS model for Ni, Fe, and Cr in steels.

Two mechanisms that can act to reduce the number of interstitials available to participate in RIS and their resulting impact on the model predictions were assessed: Cr–Cr interstitial trapping and biased defect sinks. It was determined that even with aggressive assumptions and selection of parameters, the impact of these effects is relatively small compared with the sensitivity of the model to the Cr and Ni diffusivities. In summary, while we believe that DFT and other methods are powerful tools for understanding and modeling RIS, our results demonstrate that DFT alone may not have the accuracy at this time for quantitative Ni, Fe, and Cr RIS prediction in the Ni–Fe–Cr system.

Acknowledgements

The authors would like to acknowledge Frédéric Soisson, Maylise Nastar, and Gary Was for important insights and helpful discussion. This research was conducted under appointment to the Rickover Graduate Fellowship Program and was supported financially by the DOE Nuclear Energy Research Initiative Consortium (NERI-C) award number DE-FG07-07ID14894.

References

[1] G.S. Was, Fundamentals of radiation materials science: metals and alloys, Springer, Berlin; New York, 2007.
[2] D.R. Olander, United States. Energy Research and Development Administration. Division of Reactor Development and Demonstration., Fundamental aspects of nuclear reactor fuel elements : prepared for the Division of Reactor Development and Demonstration, Energy Research and Development Administration, Technical Information Center, Office of Public Affairs. National Technical Information Service, US Dept. of Commerce, Oak Ridge, Tenn. Springfield, Va., 1976.
[3] H. Hanninen, I. Aho-Mantila, Environment-sensitive cracking of reactor internals, in: Third International Symposium on Environmental Degradation of Materials in Nuclear Power Systems – Water Reactors, The Metallurgical Society, 1988, pp. 77–92.
[4] S.M. Bruemmer, G.S. Was, J. Nucl. Mater. 216 (1994) 348–363.
[5] J.T. Busby, G.S. Was, E.A. Kenik, J. Nucl. Mater. 302 (2002) 20–40.
[6] J.M. Perks, A.D. Marwick, C.A. English, Computer code to calculate radiation induced segregation in concentrated ternary alloys, in: AERE-R-12121, 1986, p. 48.
[7] Y. Grandjean, P. Bellon, G. Martin, Physical Review B 50 (1994) 4228–4231.
[8] T.R. Allen, G.S. Was, Acta Mater. 46 (1998) 3679–3691.
[9] K. Fukuya, K. Fujii, J. Nucl. Sci. Technol. 46 (2009) 744–752.
[10] J.D. Tucker, R. Najafabadi, T.R. Allen, D. Morgan, J. Nucl. Mater. 405 (2010) 216–234.
[11] M. Nastar, P. Bellon, G. Martin, J. Ruste, Mater. Res. Soc. Symp. Proc. 481 (1998) 383–388.
[12] S. Choudhury, L. Barnard, J.D. Tucker, T.R. Allen, B.D. Wirth, M. Asta, D. Morgan, J. Nucl. Mater. 411 (2011) 1–14.
[13] F. Soisson, J. Nucl. Mater. 349 (2006) 235–250.
[14] A.R. Allnatt, A.B. Lidiard, Atomic transport in solids, Cambridge University Press, Cambridge [England]; New York, 1993.
[15] A. Van der Ven, H.C. Yu, G. Ceder, K. Thornton, Prog. Mater. Sci. (2009).
[16] K. Radhakrishnan, A. Hindmarsh, Lawrence Livermore National Laboratory Report, UCRL-ID-113855, 1993.
[17] C.H.P. Lupis, Chemical Thermodynamics of Materials, North-Holland, New York, 1983.
[18] J.R. Manning, Physical Review B 4 (1971) 1111.
[19] J.L. Bocquet, Acta Metall. 34 (1986) 571–597.
[20] T.R. Allen, L. Tan, G.S. Was, E.A. Kenik, J. Nucl. Mater. 361 (2007) 174–183.
[21] R.D. Carter, D.L. Damcott, M. Atzmon, G.S. Was, S.M. Bruemmer, E.A. Kenik, J. Nucl. Mater. 211 (1994) 70–84.
[22] J.D. Tucker, T.R. Allen, R. Najafabadi, D. Morgan, Computational Methods and Reactor Physics, M and C 2 (2009) 891–901.
[23] W.G. Wolfer, J. Computer-Aided Mater. Des. 14 (2007) 403–417.
[24] C.H. Woo, B.N. Singh, Philosophical Magazine a-Physics of Condensed Matter Structure Defects and Mechanical Properties 65 (1992) 889–912.
[25] Y.N. Osetsky, D.J. Bacon, B.N. Singh, B. Wirth, J. Nucl. Mater. 307 (2002) 852–861.
[26] N. Sakaguchi, T. Shibayama, H. Kinoshita, H. Takahashi, Philos. Mag. Lett. 81 (2001) 691–696.
[27] M.J. Hackett, R. Najafabadi, G.S. Was, J. Nucl. Mater. 389 (2009) 279–287.
[28] R.E. Reed-Hill, R. Abbaschian, Physical Metallurgy Principles, 3rd ed., PWS-Kent Pub., Boston, Mass, 1992.
[29] T.R. Allen, J.T. Busby, G.S. Was, E.A. Kenik, J. Nucl. Mater. 255 (1998) 44–58.